A Compact Circularly Polarized Multibeam Antenna Using Defected Polarization Conversion Metasurface

Qing Liu, Ming-Yao Xia, *Senior Member, IEEE*, and Wen-Mei Zhang, *Senior Member, IEEE*

***Abstract*—In this letter, a four-beam circularly polarized (CP) antenna in the Ku-band based on metasurface (MS) is proposed. It consists of a defected polarization conversion metasurface (PCM) and a feeding structure. The PCM is composed of centrosymmetric units, each of which contains a pair of square patches and a pair of L-shaped patches. When it is placed above the feeding structure, the linearly polarized (LP) wave is converted into a CP wave, and the gain is also enhanced. Furthermore, through loading stubs on the microstrip feeding lines and modifying the PCM as a defected PCM by removing some units from the MS, both the back and sidelobe levels are reduced. The realized antenna has a compact dimension of $1.05\lambda_0 \times 1.05\lambda_0 \times 0.12\lambda_0$. It has a −10 dB impedance bandwidth from 12.69 to 13.38 GHz (5.3%) and a 3 dB axial ratio bandwidth from 12.69 to 13.88 GHz (9.1%). When the four ports are excited, the four beams point at $(\theta, \phi) = (40°, 105°), (40°, 165°), (40°, 285°)$, and $(40°, 345°)$, respectively. The four beam directions may be altered by readjusting the coupling slots in the ground plane. The gain in the working band reaches 8.27 dBi.**

***Index Terms*—Circular polarization (CP), metasurface (MS), multibeam, stubs.**

I. Introduction

With the rapid growth of various wireless communication fashions, multibeam antennas (MBAs) have become an essential choice for improving the system capacity and spectrum efficiency [1], [2]. MBAs with circular polarization (CP) radiation have drawn much attention due it can reduce the multipath interference and the polarization mismatch.

Literatures offered numerous approaches for designing MBAs, one of which was the antenna array based on the Butler matrix [3], [4]. In [4], an MBA fed by a 4×4 Butler matrix was presented. The antenna achieved a high gain of 9.8 dBi. However, its horizontal dimension was as large as $20\lambda_0 \times 3\lambda_0$. Because of its large size, it is not suitable for constructing antenna arrays for base station applications. Antenna arrays fed by Butler can achieve high gain, but may have large size and high profile, which restrict its overall utility.

In another manner, MBAs may be realized through the control of beam scanning [5], [6], [7], [8]. In [6], a compact dielectric resonant scanning antenna was proposed. This antenna achieved beam steering by moving a gravitational ball lens. However, the profile of the antenna was $0.48\lambda_0$. It is too high to suit a compact base station. Besides, many beam scanning antennas require mechanical control, which would increase losses and production costs.

In addition to the above-mentioned antennas, antennas based on metasurfaces (MS) have been extensively studied because of their many advantages, including high gain and low profile [9], [10], [11], [12], [13]. In [9], the principle of phase superposition was utilized to design a four-beam CP antenna. It used a four-layer MS to achieve a phase range of 360° and a gain of 8.7 dBi. However, its size was as large as $4.25\lambda_0 \times 4.25\lambda_0$. In [12], the antenna achieved multiple beams by feeding different ports. It enhanced the beam's performance by placing a dielectric substrate above the MS. In [13], the antenna achieved multiple beams in a similar way to [12]. It suppressed sidelobes and reduced the profile by placing a high-impedance surface below the square loop antenna. The profile of the antenna was only $0.07\lambda_0$.

In order to broaden the bandwidth of multiple beams, the design of the feed source is also crucial. In [14], the antenna was fed by coaxial lines. It got 12 beams by applying different excitations to the four ports. However, the bandwidth was only 0.06 GHz. In [15], the bandwidth of the antenna was broadened to 0.47 GHz by using slot coupling feeding. It reduced the back lobe by etching a compound double annular slot on the ground.

Ku-band has the advantages of high frequency, large satellite channel capacity, and low interference. The antennas operating in this band have great potential for applications in satellite communications, vehicular communications, unmanned aerial vehicle (UAV) communications, and other fields.

In this letter, an MBA based on defected polarization conversion metasurface (PCM) is proposed to realize a four-beam CP antenna in the Ku-band. The four beam directions can be altered by shifting the coupling slots in the ground plane and the sidelobe can be reduced by adding stubs to microstrip feeding lines. The antenna attains a high gain of 8.27 dBi, while its volume is only $1.05\lambda_0 \times 1.05\lambda_0 \times 0.12\lambda_0$.

II. Antenna Configuration

Fig. 1 shows the geometry of the MBA with CP radiation proposed in this letter. The substrate is PTFE with relative permittivity of 2.2 and loss tangent of 0.002. The antenna includes a feeding source and a MS separated by an air layer with a height of h_c. The centrosymmetric MS units are etched on the substrate 1, each of which consists of a pair of square patches and a pair of L-shaped patches, which is merged with adjacent square patches [To show the connection between the units, a

Manuscript received 22 March 2023; accepted 13 April 2023. Date of publication 21 April 2023; date of current version 4 August 2023. This work was supported in part by the National Science Foundation of China (62071282), in part by the National Science Foundation of Shanxi Province (202203021211295); and in part by "Shanxi" "1331" "Project" Key Subjects Construction [1331KSC]. *(Corresponding author: Wen-Mei Zhang.)*

Qing Liu and Wen-Mei Zhang are with the School of Physics and Electronic Engineering, Shanxi University, Shanxi 030006, China (e-mail: lqq011994@163.com; zhangwm@sxu.edu.cn).

Ming-Yao Xia is with the School of Electronics, Peking University, Beijing 100871, China (e-mail: myxia@pku.edu.cn).

Digital Object Identifier 10.1109/LAWP.2023.3269049

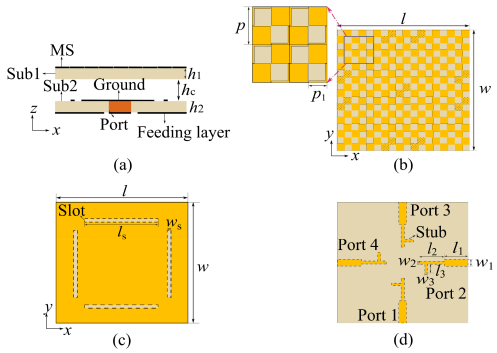

Fig. 1. Structure of the antenna. (a) Side view. (b) MS. (c) Ground plane with etched slots. (d) Four microstrip lines.

TABLE I
STRUCTURE PARAMETER OF THE ANTENNA

Symbol	Value(mm)	Symbol	Value(mm)	Symbol	Value(mm)
l	23.6	l_1	4.3	w_3	0.5
w	23.6	w_1	1.4	l_s	11.8
p_1	1.19	l_2	4.5	w_s	0.4
p	2.4	w_2	0.6	h_1	1
h_c	1	l_3	1.7	h_2	1

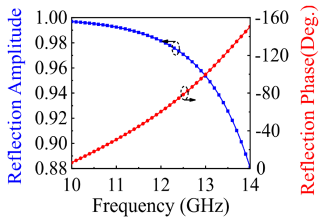

Fig. 2. Simulated reflection amplitude and phase of an MS unit.

2 × 2 unit is displayed in Fig. 1(b)]. The units are arranged symmetrically along the 45° and 135° directions. To improve the radiation performance, the nine dotted units (two above each of the four ports, and one near the center) are removed to make the PCM become a defected PCM.

The feeding structure is printed on the lower side of substrate 2. On its upper side, the ground plane is etched with four rectangular slots, as displayed in Fig. 1(c). The four microstrip lines with tuning stubs on the lower side are shown in Fig. 1(d). An antenna operating at 13 GHz is designed to verify the idea, and the dimensions are given in Table I.

III. MULTIBEAM FORMING TECHNOLOGY

In this section, detailed designs of the antenna are addressed.

A. Refection Property of a Unit and the Cavity Height

First, the refection property of an isolated unit is simulated with CST, and the results are shown in Fig. 2. In the frequency range of 10–14 GHz, its amplitude A_r is changed from 1 to 0.88. At 13 GHz, $A_r = 0.95$. Therefore, the PCM is used as a partially reflective surface. Then, a resonator cavity is designed. The waves will have an in-phase superposition in the resonant cavity when the height of the air layer h_c meets

$$hc + h1 = (\varphi_{MS} + \varphi_g)\frac{\lambda}{4\pi} \pm N\frac{\lambda}{2} \quad (N = 0, 1, 2, 3, \ldots) \quad (1)$$

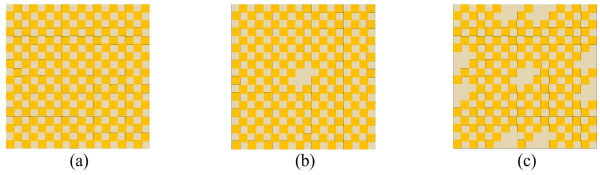

Fig. 3. Design process of the PCM. (a) Uniform PCM. (b) PCM with center unit removed. (c) Designed PCM.

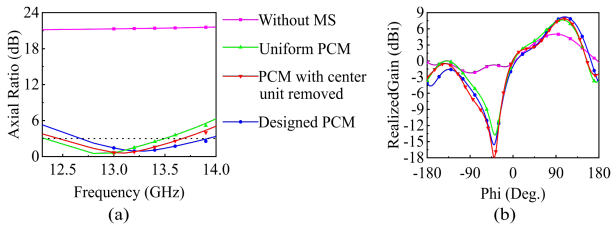

Fig. 4 Simulated results. (a) Axial ratios. (b) Gain patterns in the $\theta = 40°$ conical surface.

where, $\varphi_{\rm MS}$ and $\varphi_{\rm g}$ represent the reflection phase of the MS and the ground plane, respectively, λ is the wavelength in free space. As shown in Fig. 2, $\varphi_{\rm MS} = -99.74°$. Taking $\varphi_{\rm g} = 180°$ and $N = 0$, we get $h_c + h_1 \approx 2.6$ mm by (1). Therefore, the height h_c of the air layer should be $h_c \approx 1.6$ mm. After overall optimization considering the couplings between the units, the h_c is finally determined to be 1 mm.

B. Effect of Defected MS

To clearly explain the design process, three PCM are examined, as shown in Fig. 3. Comparisons of axis ratio (AR) and gain of antennas loaded with three different PCM are shown in Fig. 4. For comparison, results for the antenna without MS are also provided. For antenna without MS, it radiates LP waves, and its main beam appears around 105° with a gain of 5 dBi. In order to improve the gain, Fig. 3(a) is loaded with a uniform PCM. As a result, the gain is increased to 7.6 dBi. At the meantime, it produces a CP radiation with 3 dB AR bandwidth from 12.25 to 13.5 GHz. However, its sidelobe is obvious. In this case, by removing the center position of the PCM, we get the Fig. 3(b), so that the sidelobe is reduced from 0 dB to −0.5 dB. Moreover, its AR bandwidth moves to higher band. To further improve the radiation characteristic, more units are removed to get the Fig. 3(c), in which two units above each port are removed, and the side lobe is reduced from −0.5 dB to −1.99 dB. Meanwhile, the gain is enhanced from 7.7 dBi to 8.27 dBi. In addition, operating bands of AR < 3 dB continue to move toward higher bands. Fig. 3(c) is the final design of the defected PCM. Actually, we have tried to change the positions of the nine units to be removed, and Fig. 3(c) seems to be the best choice.

Regarding the size of the MS, Fig. 5 shows the changes in realized gains when the number of units is increased from 4×4 to 9 × 9. It can be seen that the gain is increased from 5.75 to 8.27 dBi, whereas the sidelobe is decreased from 0.31 dB to −4.9 dB. It seems unnecessary to continue increasing the size.

C. Theory of Polarization Conversion

An equivalent circuit is employed to explain the polarization conversion mechanism of PCM. As shown in Fig. 6(a), a single

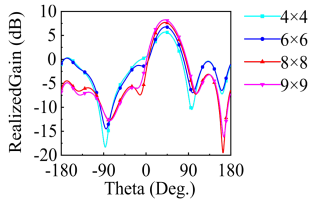

Fig. 5. Realized gains with different size MS.

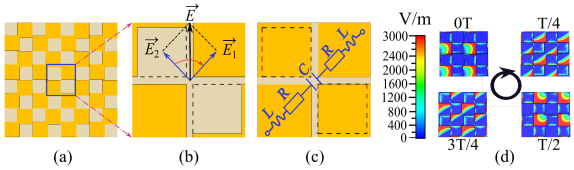

Fig. 6. Equivalent circuit analysis. (a) MS. (b) Unit cell with diagonal patches cutoff. (c) Unit cell without diagonal patches cutoff. (d) Electric field distribution at four moments in PCM.

unit cell may be taken out to account for the point, whose enlarged version is displayed in Fig. 6(b). Before the two diagonal patches are cut off, as shown in Fig. 6(c), each pair of diagonal patches can be regarded as a symmetric RLC circuit, and its impedance along the $\vec{E}_1$ direction is

$$Z_1 = 2R + j\omega(2L) + \frac{1}{j\omega C} = R_1 + jX_1 \tag{2}$$

where R and L are, respectively, the equivalent resistance and inductance of one patch, and C is the capacitance formed by the gap between the opposite patches. When port 1 is excited, each pair of diagonal patches radiates a LP wave along the $\vec{E}_1$ and $\vec{E}_2$ directions, respectively. Because of symmetry, the two pairs of diagonal patches will radiate a y-polarized LP wave.

After a pair of diagonal patches are cutoff, the amplitude and/or phase of $\vec{E}_2$ radiated by the slots would differ from those of $\vec{E}_1$. The equivalent impedance corresponding to $\vec{E}_2$ changes to

$$Z_2 = R_2 + jX_2 \tag{3}$$

which is adjustable by the size of truncation. If the MS is designed so that $|Z_2| = |Z_1|$ and $\angle Z_2 - \angle Z_1 = 90^o$, then $|\vec{E}_2| = |\vec{E}_1|$ and $\angle\vec{E}_2 - \angle\vec{E}_1 = 90^o$, $\vec{E}_2$ will lead $\vec{E}_1$ by 90° and the left-handed circular polarization (LHCP) will be created, as represented by the red arc arrow in Fig. 6(b). Similarly, to reconfigure the antenna to right-handed circular polarization (RHCP), we can excite port 2, so that the value of X_2 in (2) becomes larger and $\vec{E}_1$ will lead $\vec{E}_2$ by 90°.

To help in understanding the physical significance of the antenna operation, in general, in Fig. 6(d), the electric field distributions on PCM during a period T are displayed. It shows that the electric field rotates clockwise, which generates a LHCP radiation in this band.

D. Contribution of Stubs

Stubs loaded on feeding lines also contribute to improve the radiation performance of antenna. Without losing generality, the improvement mechanism can be discussed by analyzing the current distributions for port 1 as displayed in Fig. 7. It can be seen that the current at the end of port 1 is reduced with loading

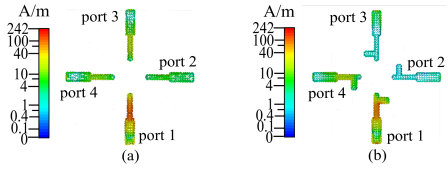

Fig. 7. Current distributions on the four feeding lines when the port 1 is excited. (a) Without stubs and (b) with stubs.

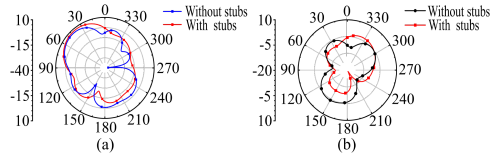

Fig. 8. Gain patterns of the antenna without and with stubs in the plane of (a) $\phi = 105°$ and (b) $\phi = 195°$.

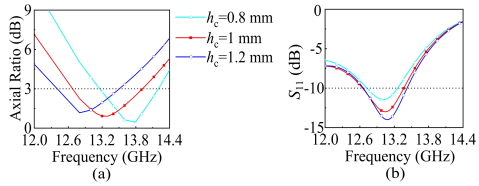

Fig. 9. Antenna performance changes with h_c. (a) AR. (b) Impedance matching.

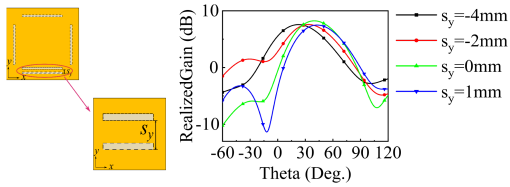

Fig. 10. Control the beam direction in elevation plane by adjusting s_y.

the stubs. So, the current coupled to other ports is cut down. As a result, the gain patterns in the plane of $\phi = 105°$ and $\phi = 195°$ is shown in Fig. 8. It indicates that the sidelobe around (35°, 195°) is reduced from −0.6 to −4.3 dB, and the backward radiation around (145°, 195°) is decreased from 0.77 to −5.93 dB. Also, the gain of the antenna is increased from 7.49 to 8.27 dBi.

E. Selection of H_c

The height of the air layer has a great influence on the operating band of the antenna, as shown in Fig. 9. As h_c increases from 0.8 to 1.2 mm, the frequency band of AR < 3 dB is reduced. While the center frequency for $S_{11} < 10$ dB is basically unchanged. Therefore, to obtain identical band for impedance matching and AR, the $h_c = 1$ mm is selected.

F. Steering Beam in Elevation Plane

The direction of beam may be changed by adjusting the position of the slot on the ground. As shown in Fig. 10, for the slot above port 1, by moving it from −4 to 1 mm in the y direction (from the edge to center of MS), the elevation angle θ will increases from 20° to 45°. The details of the data are given in Table II.

TABLE II
RADIATION PERFORMANCE OF DIFFERENT s_Y

s_y(mm)	-4	-2	0	1
(φ, θ)	115°, 20°	85°, 30°	105°, 40°	115°, 45°

TABLE III
PHASE DISTRIBUTION FOR DIFFERENT s_Y

s_y(mm)	y (mm)								$\triangle\varphi$	θ
	-9.6	-7.2	-4.8	-2.4	2.4	4.8	7.2	9.6	(deg.)	(deg.)
-4	223.4	359.4	31.3	358.4	148.2	237.1	315.8	353.1	18.5	19.4
-2	167.3	359.3	22.6	313.1	125.7	265.5	323.6	359.9	27.5	29.5
0	116.9	359.8	23.4	291.8	123.2	256.7	336.2	359.2	34.6	38.3
1	87.8	356.8	36.3	316.1	134.4	243.7	329.9	357.5	38.5	43.5

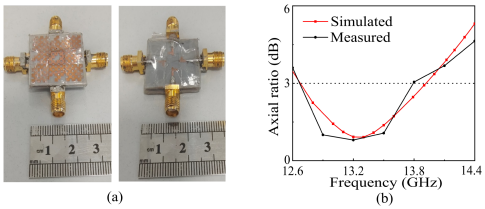

Fig. 11. Photos of fabricated and its AR. (a) Photographs of antenna. (b) Simulated and measured AR of the antenna.

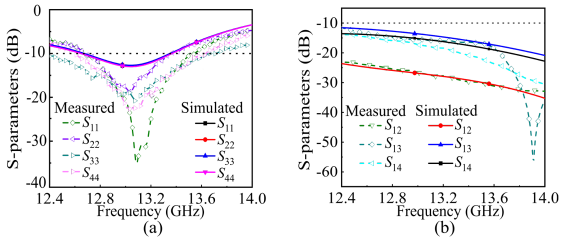

Fig. 12. Measured S-parameters of the antenna. (a) Reflection parameters. (b) Isolation.

Here, the phase distribution is recorded for different s_y at 13 GHz and listed in Table III. The theoretical beam deflection angle θ is obtained as

$$\sin\theta = \frac{\lambda_g \Delta\varphi}{2\pi p} \tag{4}$$

where λ_g is the wavelength of guided wave, p is the period of the defected PCM unit, and $\Delta\varphi$ is the average phase delay of eight observation points. As can be seen from Table III, the beam θ calculated by (4) is close to the simulated results.

IV. SIMULATED AND MEASURED RESULTS

To verify the proposed design, a prototype of the antenna as shown in Fig. 11(a) is fabricated and measured. Its simulated and measured AR is displayed in Fig. 11(b). The simulated result of the 3 dB AR relative bandwidth is 9.1% (12.69–13.88 GHz), whereas the measured result is 8.9% (12.66–13.82 GHz).

Fig. 12 shows the simulated and measured S-parameters. As the overall structure of the antenna is centrosymmetric, only the results for port 1 are given. In Fig. 12(a), the measured S_{11} curve has the same variation trend with the simulated one. The simulated impedance bandwidth is 0.69 GHz (12.69–13.38 GHz), and the measured results of the four ports are in the ranges of 12.7–13.6 GHz, 12.7–13.4 GHz, 12.4–13.7 GHz, and 12.6–13.6 GHz, respectively. As displayed in Fig. 12(b), the isolations are better than 12 dB.

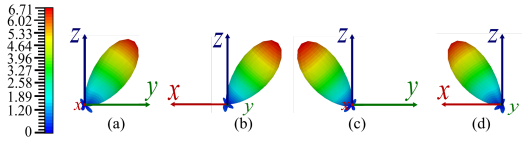

Fig. 13. Four beams of the antenna at 13 GHz. (a) Port 1. (b) Port 2. (c) Port 3. (d) Port 4.

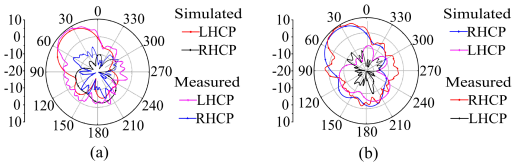

Fig. 14. Radiation patterns of the antenna. (a) By exciting port 1/3. (b) By exciting port 2/4.

TABLE IV
COMPARISONS OF CP RADIATION MBA

Ref.	Feeding structure	Dimension(λ_0^3)	Pol.	Beam coverage	Gain (dBi)
[3]	4-port	22×2.32×0.24	CP	±15° ±45°	7.4
[4]	8-port	20×3×0.38	Dual-CP	±16° ±38°	9.8
[5]	1-port	2.9×2.8×0.36	CP	0° -15° -30° -45°	10.5
[6]	2-port	0.58×0.58×0.48	Dual-CP	0° ±20° ±50°	4.9
[9]	1-port	4.25×4.25×0.75	CP	0° 90° 180° 270°	8.7
This work	4-port	1.05×1.05×0.12	Dual-CP	105° 165° 285° 345°	8.27

Abbreviation: λ_0, the wavelength at the center frequency.

Figs. 13 and 14 display the 3-D and 2-D radiation patterns at 13 GHz. In Fig. 13, when ports 1–4 are excited, four beams point at $(\theta, \phi) = (40°, 105°)$, $(40°, 165°)$, $(40°, 285°)$, and $(40°, 345°)$, respectively. In Fig. 14, antenna radiates LHCP by exciting port 1 or 3 and radiates RHCP in the case of exciting port 2 or 4. The measured angle between the radiation beams and the z-axis is 40°. In addition, the measured differences between the copolarization and the cross polarization are 16.48 and 20 dB in Fig. 14(a) and (b), less than the simulated results.

Finally, the four-beam antenna with CP radiation proposed is compared with other MBAs, as given in Table IV. The proposed antenna achieves a higher gain in a more compact volume.

V. CONCLUSION

In this letter, a compact four-beam with CP radiation antenna based on defected PCM is designed. The four beams point at $(\theta, \phi) = (40°, 105°)$, $(40°, 165°)$, $(40°, 285°)$, and $(40°, 345°)$, respectively. The beam directions may be changed by adjusting the positions of coupling slots. The -10 dB impedance bandwidth is from 12.69 to 13.38 GHz, and the 3 dB AR bandwidth is from 12.69 to 13.88 GHz. Through loading tuning stubs on the microstrip feeding lines, both the back lobe and sidelobe level (SLL) of the antenna are reduced. The gain of the antenna is up to 8.27 dBi despite the small size of $1.05\lambda_0 \times 1.05\lambda_0 \times 0.12\lambda_0$. The antenna may be used as base station or mobile antenna to cover four fixed areas.

REFERENCES

[1] W. Hong et al., "Multibeam antenna technologies for 5G wireless communications," *IEEE Trans. Antennas Propag.*, vol. 65, no. 12, pp. 6231–6249, Dec. 2017.

[2] D. Peng, D. He, Y. Li, and Z. Wang, "Integrating terrestrial and satellite multibeam systems toward 6G: Techniques and challenges for interference mitigation," *IEEE Wireless Commun.*, vol. 29, no. 1, pp. 24–31, Feb. 2022.

[3] F. Y. Xia, Y. J. Cheng, Y. F. Wu, and Y. Fan, "*V*-band wideband circularly polarized end-fire multibeam antenna with wide beam coverage," *IEEE Antennas Wireless Propag. Lett.*, vol. 18, no. 8, pp. 1616–1620, Aug. 2019.

[4] Q. Wu, J. Hirokawa, J. Yin, C. Yu, H. Wang, and W. Hong, "Millimeter-wave multibeam endfire dual-circularly polarized antenna array for 5G wireless applications," *IEEE Trans. Antennas Propag.*, vol. 66, no. 9, pp. 4930–4935, Sep. 2018.

[5] K. Al-Amoodi, M. M. Honari, R. Mirzavand, J. Melzer, D. G. Elliott, and P. Mousavi, "Circularly-polarised end-fire antenna and arrays for 5G millimetre-wave beam-steering systems," *Microw., Antennas Propag.*, vol. 14, no. 9, pp. 980–987, May 2020.

[6] Z. Chen, Q. Liu, B. Sanz-Izquierdo, H. Liu, J. Yu, and X. Chen, "A wideband circular-polarized beam steering dielectric resonator antenna using gravitational ball lens," *IEEE Trans. Antennas Propag.*, vol. 69, no. 5, pp. 2963–2968, May 2021.

[7] A. H. Naqvi and S. Lim, "A beam-steering antenna with a fluidically programmable metasurface," *IEEE Trans. Antennas Propag.*, vol. 67, no. 6, pp. 3704–3711, Jun. 2019.

[8] K. K. Katare, S. Chandravanshi, A. Biswas, and M. J. Akhtar, "Beam-switching of Fabry–Perot cavity antenna using asymmetric reflection phase response of bianisotropic metasurface," *Microw., Antennas Propag.*, vol. 13, no. 6, pp. 842–848, Mar. 2019.

[9] C.-H. Lee, T. V. Hoang, S. W. Chi, S.-G. Lee, and J.-H. Lee, "Low profile quad-beam circularly polarized antenna using transmissive metasurface," *Microw., Antennas Propag.*, vol. 13, no. 10, pp. 1690–1698, May 2019.

[10] W. Zhang, A. Pal, A. Mehta, D. Mirshekar-Syahkai, and H. Nakano, "Low profile pattern-switchable multibeam antenna consisting of four L-shaped microstrip lines," *Microw., Antennas Propag.*, vol. 12, no. 11, pp. 1846–1851, May 2018.

[11] J. Luo, L. Li, J. Su, R. Ma, G. Han, and W. Zhang, "Multibeam antenna based on partially reflecting defected metasurface," *IEEE Antennas Wireless Propag. Lett.*, vol. 20, no. 8, pp. 1582–1586, Aug. 2021.

[12] J. Zhang, L. Han, X. Chen, R. Yang, and W. Zhang, "Multi-beam patch antenna based on metasurface," *IEEE Access*, vol. 8, pp. 37281–37286, 2020.

[13] P. Deo, A. Mehta, D. Mirshekar-Syahkal, P. J. Massey, and H. Nakano, "Thickness reduction and performance enhancement of steerable square loop antenna using hybrid high impedance surface," *IEEE Trans. Antennas Propag.*, vol. 58, no. 5, pp. 1477–1485, May 2010.

[14] A. Pal, A. Mehta, D. Mirshekar-Syahkal, and H. Nakano, "A twelve-beam steering low-profile patch antenna with shorting vias for vehicular applications," *IEEE Trans. Antennas Propag.*, vol. 65, no. 8, pp. 3905–3912, Aug. 2017.

[15] Z. Zhao and W. Zhang, "Multi-beam antenna based on annular slot and uneven metasurface," *Int. J. RF Microw. Comput.-Aided Eng.*, vol. 31, no. 11, Jul. 2021, Art. no. e22814.